The Plant Cell, Vol. 28: 1844–1859, August 2016, www.plantcell.org

SHORT-ROOT Deficiency Alleviates the Cell Death Phenotype of the *Arabidopsis catalase2* Mutant under Photorespiration-Promoting Conditions

Cezary Waszczak,[a,b,c,d,e,f,1] Pavel I. Kerchev,[a,b,1] Per Mühlenbock,[a,b,2] Frank A. Hoeberichts,[a,b,3] Katrien Van Der Kelen,[a,b] Amna Mhamdi,[a,b,g,h] Patrick Willems,[a,b] Jordi Denecker,[a,b,4] Robert P. Kumpf,[a,b] Graham Noctor,[g,h] Joris Messens,[c,d,e] and Frank Van Breusegem[a,b,5]

[a] Department of Plant Systems Biology, VIB, 9052 Ghent, Belgium
[b] Department of Plant Biotechnology and Bioinformatics, Ghent University, 9052 Ghent, Belgium
[c] Structural Biology Research Center, VIB, 1050 Brussels, Belgium
[d] Structural Biology Brussels Laboratory, Vrije Universiteit Brussel, 1050 Brussels, Belgium
[e] Brussels Center for Redox Biology, 1050 Brussels, Belgium
[f] Division of Plant Biology, Department of Biosciences, Viikki Plant Science Center, University of Helsinki, FI-00014 Helsinki, Finland
[g] Institute of Plant Sciences Paris Saclay IPS2, CNRS, INRA, Université Paris-Sud, Université Evry, Université Paris-Saclay, 91405 Orsay, France
[h] Institute of Plant Sciences Paris-Saclay IPS2, Paris Diderot, Sorbonne Paris-Cité, 91405 Orsay, France

ORCID IDs: 0000-0003-2737-0493 (P.I.K.); 0000-0003-3097-8387 (P.M.); 0000-0001-9959-1362 (A.M.); 0000-0003-4667-2294 (P.W.); 0000-0003-1980-4554 (G.N.); 0000-0002-2128-8264 (J.M.); 0000-0002-3147-0860 (F.V.B.)

Hydrogen peroxide (H_2O_2) can act as a signaling molecule that influences various aspects of plant growth and development, including stress signaling and cell death. To analyze molecular mechanisms that regulate the response to increased H_2O_2 levels in plant cells, we focused on the photorespiration-dependent peroxisomal H_2O_2 production in *Arabidopsis thaliana* mutants lacking CATALASE2 (CAT2) activity (*cat2-2*). By screening for second-site mutations that attenuate the PSII maximum efficiency (F_v'/F_m') decrease and lesion formation linked to the *cat2-2* phenotype, we discovered that a mutation in SHORT-ROOT (SHR) rescued the cell death phenotype of *cat2-2* plants under photorespiration-promoting conditions. SHR deficiency attenuated H_2O_2-dependent gene expression, oxidation of the glutathione pool, and ascorbate depletion in a *cat2-2* genetic background upon exposure to photorespiratory stress. Decreased glycolate oxidase and catalase activities together with accumulation of glycolate further implied that SHR deficiency impacts the cellular redox homeostasis by limiting peroxisomal H_2O_2 production. The photorespiratory phenotype of *cat2-2* mutants did not depend on the SHR functional interactor SCARECROW and the sugar signaling component ABSCISIC ACID INSENSITIVE4, despite the requirement for exogenous sucrose for cell death attenuation in *cat2-2 shr-6* double mutants. Our findings reveal a link between SHR and photorespiratory H_2O_2 production that has implications for the integration of developmental and stress responses.

INTRODUCTION

In plants, numerous growth, developmental, and defense-related processes rely on redox homeostasis, which is maintained by an extensive antioxidant machinery (Schürmann and Buchanan, 2008; Foyer and Noctor, 2009; Van den Ende and Valluru, 2009; Mittler et al., 2011; Considine and Foyer, 2014). The composition of the antioxidant system in each cellular compartment reflects the need for removal of the respective forms and amounts of reactive oxygen species (ROS). For example, because peroxisomal reactions generate substantial amounts of hydrogen peroxide (H_2O_2), peroxisomes contain catalase that converts H_2O_2 into water and oxygen. In photosynthetic cells, catalase decomposes the H_2O_2 generated as glycolate is oxidized to glyoxylate by glycolate oxidase (GOX). The peroxisomal H_2O_2-scavenging system minimizes the oxidative damage to vulnerable cellular constituents and the failure to dissipate photorespiratory H_2O_2 triggers redox signaling pathways (Mhamdi et al., 2012; Sandalio and Romero-Puertas, 2015). Among the ROS, H_2O_2 has the highest potential to act as a signaling molecule because of its relative stability, ability to cross membranes (Bienert et al., 2007; Tian et al., 2016), and role in posttranslational modification of cysteine and methionine residues in target proteins (Waszczak et al., 2014, 2015; Jacques et al., 2015).

Arabidopsis thaliana plants that lack peroxisomal catalase have been extensively used as a model system to mimic increased endogenous H_2O_2 levels in a noninvasive, physiologically relevant

[1] These authors contributed equally to this work.
[2] Current address: PhotonFate AB, 147 33 Tumba, Sweden.
[3] Current address: NSure, 6709 PD Wageningen, The Netherlands.
[4] Current address: Illumina United Kingdom–Fulbourn, Cambridge CB21 5XE, UK.
[5] Address correspondence to frank.vanbreusegem@psb.vib-ugent.be.
The author responsible for distribution of materials integral to the findings presented in this article in accordance with the policy described in the Instructions for Authors (www.plantcell.org) is: Frank Van Breusegem (frank.vanbreusegem@psb.vib-ugent.be).
www.plantcell.org/cgi/doi/10.1105/tpc.16.00038

manner (Vandenabeele et al., 2004; Vanderauwera et al., 2005; Queval et al., 2007; Mhamdi et al., 2010; Noctor et al., 2015). When grown under ambient air and moderate light intensities, *cat2* mutant plants, which are deficient in CATALASE2, display photoperiod-dependent morphological characteristics, such as stunted rosettes and lesion formation (Queval et al., 2007). Moreover, these growth conditions lead to accumulation of oxidized glutathione, reflecting a general disturbance of the redox homeostasis (Queval et al., 2007; Chaouch et al., 2010). As these phenotypes are not observed under conditions that limit the flux through the photorespiratory pathway (such as high CO_2 levels), they are classified as conditional. Therefore, *cat2* requires elevated CO_2 concentrations for proper growth and development (Queval et al., 2007). Second-site mutations that alleviate the photorespiratory phenotype of *cat2* are instrumental in elucidating peroxisomal H_2O_2-triggered signaling events (Kaurilind et al., 2015). Lesions induced by peroxisomal H_2O_2 are abolished in double mutants that lack the salicylic acid (SA) biosynthetic enzyme ISOCHORISMATE SYNTHASE1, implying a role for SA accumulation in the photorespiratory phenotype of *cat2* (Chaouch et al., 2010). An alternative mechanism that attenuates cell death in *cat2* mutants was revealed by introducing a loss-of-function allele of cytosolic ASCORBATE PEROXIDASE1 (APX1) into the *cat2* background. The simultaneous loss of both enzymes constitutively activates a DNA damage response that is accompanied by enhanced oxidative stress tolerance (Vanderauwera et al., 2011). On the contrary, a *cat2-2 pp2a-β′γ* double mutant exhibits intensified SA responses and lesion formation (Li et al., 2014), demonstrating that the type 2A protein phosphatase subunit PP2A-β′γ is a negative regulator of the peroxisomal H_2O_2-induced responses.

The SHORT-ROOT (SHR) transcription factor was initially identified as a transcriptional regulator required for adequate growth and radial patterning of roots. Null *shr* mutants exhibit premature termination of root growth, resulting from a disorganized quiescent center and consequent loss of stem cell activity (Benfey et al., 1993; Scheres et al., 1995; Helariutta et al., 2000). Moreover, *shr* plants display a severely dwarfed shoot phenotype that is independent from the impaired root development (Dhondt et al., 2010). In leaf cells, SHR deficiency triggers an earlier exit from the proliferation phase that is associated with a premature decrease in expression of cell cycle regulators (Dhondt et al., 2010). Furthermore, SHR is crucial for the development of bundle sheath cells in Arabidopsis (Cui et al., 2014) and was proposed to function in the formation of the Kranz-type anatomy in maize (*Zea mays*; Slewinski et al., 2012; Wang et al., 2013).

Although *SHR* expression in the root is confined to the vascular tissue, SHR migrates to the adjacent cell layers, where it, in a complex with the SCARECROW (SCR) transcription factor, is sequestered to the nucleus. This SHR-SCR interaction restricts the SHR movement and is crucial for the development of a single endodermis layer (Nakajima et al., 2001; Cui et al., 2007). The SHR-SCR complex positively regulates *SCR* expression by direct binding to the *SCR* promoter. Consequently, *SCR* transcript levels are reduced in *shr* plants with a marked overlap between the root and shoot phenotypes, including perturbed bundle sheath formation (Cui et al., 2014) and transcriptome profiles of *shr* and *scr* mutants (Scheres et al., 1995; Di Laurenzio et al., 1996; Levesque et al., 2006; Dhondt et al., 2010).

In addition to developmental cues, SHR and SCR regulate a number of genes involved in stress responses, suggesting that SHR might act as a dual regulator that regulates organ growth, while suppressing stress responses (Cui et al., 2012). Both *shr* and *scr* mutants display hypersensitivity to abscisic acid and high (4%) glucose in germination assays. Furthermore, they are impaired in starch mobilization and overaccumulate soluble sugars (Cui et al., 2012, 2014).

By screening a mutagenized population of *cat2-2* plants for second-site mutations that attenuate the induction of cell death under photorespiration-promoting conditions, we identified a loss-of-function mutation in *SHR*. Upon exposure to photorespiration-promoting conditions, mutants lacking SHR maintained a more reduced redox environment that, together with perturbations of the photorespiratory metabolism, suggested a decreased peroxisomal H_2O_2 production. The cell death attenuation was independent of the SHR functional interactor SCR. Taken together, our findings show that SHR acts as a regulator of the photorespiratory redox homeostasis that integrates stress responses and development.

RESULTS

An *SHR* Loss-of-Function Mutation Alleviates the Cell Death Phenotype of *cat2-2* Mutants under Photorespiration-Promoting Conditions

Environmental conditions enhancing the photorespiratory flux trigger peroxisomal H_2O_2 production and ultimately lead to cell death in Arabidopsis mutants lacking peroxisomal CAT2 (*cat2*) (Queval et al., 2007). In a screen for second-site mutations that alleviate the photorespiratory phenotype of *cat2-2* plants, photorespiration was promoted by restricting the ambient air influx to in vitro grown plants by sealing the Petri dishes with multiple layers of Parafilm and exposure to continuous light to avoid the influence of night respiration on gas homeostasis. As a result, the CO_2 levels in the plates decreased rapidly, enhancing the flux through the photorespiratory pathway (Vanderauwera et al., 2012; Kerchev et al., 2015). During the treatment, the PSII maximum efficiency (F_v'/F_m') was monitored as a noninvasive readout of the stress tolerance. The spatial distribution of F_v'/F_m' values is represented with a color scale ranging from black ($F_v'/F_m' = 0.0$) to white ($F_v'/F_m' = 1.0$) with red, orange, yellow, blue, and violet to purple in between. In *cat2-2* plants, the exposure to photorespiration-promoting conditions led to a gradual reduction of the PSII maximum efficiency (F_v'/F_m'), lesion formation, and complete mortality within 7 d. By contrast, wild-type Col-0 plants exhibited only a moderate decrease in F_v'/F_m' and survived the treatment (Figure 1A). In this bioassay, we screened an EMS-mutagenized *cat2-2* population of 113,000 M2 plants for mutants with a reduced F_v'/F_m' decline and attenuated cell death (Figure 1B; Supplemental Figure 1). One of the identified *cat2-2* revertants (hereafter referred to as *378.3*) was characterized further (Figures 2A to 2D) and the causative mutation was mapped to the *SHR* coding sequence (Figure 2E). Introduction of a null *shr-6* allele (a T-DNA knockout) into the *cat2-2* background was sufficient to delay cell death relative to the parental *cat2-2* single mutants in photorespiration-promoting conditions (Figures 2F and 2G). The photorespiratory

phenotype of plants heterozygous for *shr-6* in the *cat2-2* background was identical to that of *cat2-2* mutants, implying that a complete loss of SHR is required for improved survival under photorespiration-promoting conditions (Supplemental Figure 2). Interestingly, under these conditions, two independent *shr* alleles, *shr-6* and *shr-2*, retained higher F_v'/F_m' values than the wild types (Supplemental Figure 3).

Cell Death Attenuation under Photorespiratory Conditions Is Modulated by Exogenous Sugar

Given that the *378.3* mutant was discovered in a screen performed within an in vitro experimental system, we investigated whether SHR deficiency could similarly alleviate the cell death phenotype of *cat2-2* mutants in soil. Plants were grown under a high CO_2 atmosphere (3000 μL L^{-1}) to minimize the flux via the photorespiratory pathway. Photorespiratory stress was imposed by a transfer to high light (1000 μmol m^{-2} s^{-1}) and ambient air. These conditions triggered a drastic F_v'/F_m' reduction in *cat2-2* mutants (Figure 3) associated with formation of lesions that were mostly visible at the tips of mature rosette leaves, with young emerging leaves being largely unaffected (Figure 3). The combined effect of *shr-6* and *cat2-2* in the *cat2-2 shr-6* double mutants did not affect lesion development when compared with *cat2-2* plants (Figure 3).

Because the mutant screen was conducted in the presence of sucrose (1% w/v), we tested whether the presence or absence of sugar affects the *cat2-2 shr-6* phenotype and might underlie the different outcomes observed in vitro and in soil. To circumvent the growth abnormalities observed in SHR-deficient plants in the absence of sugar (Supplemental Figure 4; Cui et al., 2012), 18-d-old plants were transferred from a medium containing sucrose (1% w/v) to a sucrose-free medium and were then exposed to photorespiration-promoting conditions 3 d later. Under these conditions, the beneficial effects of the SHR deficiency (i.e., delayed cell death and moderate decrease in F_v'/F_m') were abolished, and the *cat2-2 shr-6* double mutants exhibited higher sensitivity toward the stress treatment than the *cat2-2* plants (Figure 4). Moreover, when the photorespiratory phenotype of single *shr-6* mutants was assessed after transfer to a sucrose-free medium, they displayed a cell death phenotype comparable to that of *cat2-2*, which is in contrast to their superior performance in the presence of sugar (Figure 4).

Loss of SHR Function Attenuates H_2O_2-Triggered Redox Perturbation and Gene Expression

Factors negatively affecting photorespiratory H_2O_2 accumulation are expected to increase the survival rates of *cat2-2* mutants under photorespiration-promoting conditions. The highly reactive nature of H_2O_2, however, impedes its accurate and reliable quantification. Therefore, we quantified levels of the key redox buffers GSH/GSSG and ascorbate (AA)/dehydroascorbate and performed an RNA-seq-based transcriptomic analysis of ROS-responsive genes (Figure 5; Supplemental Data Set 1). The combination of these biochemical and transcriptome data provide a good indication of the cellular redox homeostasis and is considered a reliable proxy for H_2O_2 metabolism and signaling.

GSSG accumulated significantly in *cat2-2* mutants exposed to photorespiration-promoting conditions, whereas this increase was attenuated in *cat2-2 shr-6* double mutants (Figure 5A). Similarly, the introduction of *shr-6* diminished the AA depletion observed in stressed *cat2-2* single mutants. Strikingly, the total glutathione content and its oxidation status in *shr-6* mutants were not affected by the treatment. Moreover, single *shr-6* mutants had

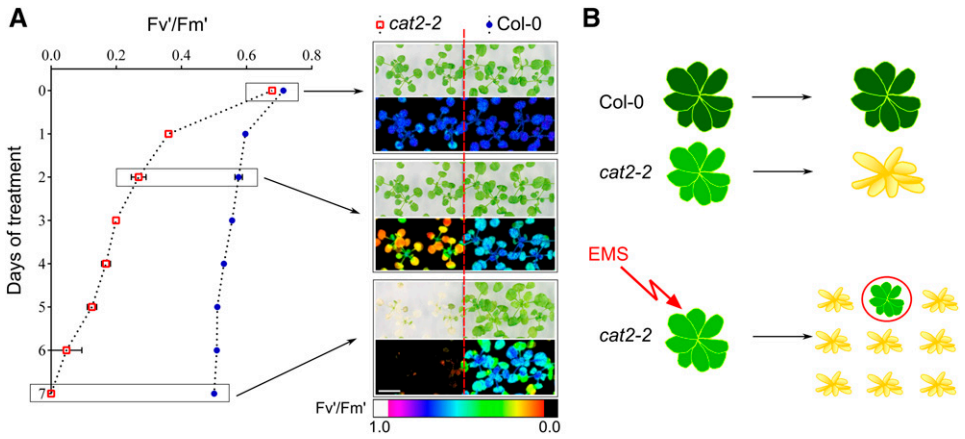

Figure 1. Strategy to Identify Second-Site Mutations That Alleviate the Photorespiratory Phenotype of *cat2-2* Mutants.

(A) PSII maximum efficiency (F_v'/F_m') decrease and cell death progression in 3-week-old plants exposed to photorespiration-promoting conditions (air-tight sealing of Petri dishes with Parafilm and transfer to continuous light). Data points represent F_v'/F_m' means from three biological replicates ±SE for *cat2-2* (red squares) and Col-0 (blue dots). Representative bright-field and color-coded images of F_v'/F_m' taken in parallel on days 0, 2, and 7 of the treatment are shown on the right. The F_v'/F_m' parameter was visualized with the use of a color scale ranging from black (0.0) to white (1.0) with red, orange, yellow, green, blue, and violet in between. Bar = 10 mm.

(B) Schematic depiction of the forward genetic screen used to identify revertants of the photorespiratory *cat2-2* phenotype. An EMS-mutagenized *cat2-2* population (113,000 M2 plants) was screened under photorespiration-promoting conditions (arrows). Plants that showed lower rates of F_v'/F_m' decrease and attenuated cell death relative to the parental *cat2-2* plants (red circle) were selected for further characterization.

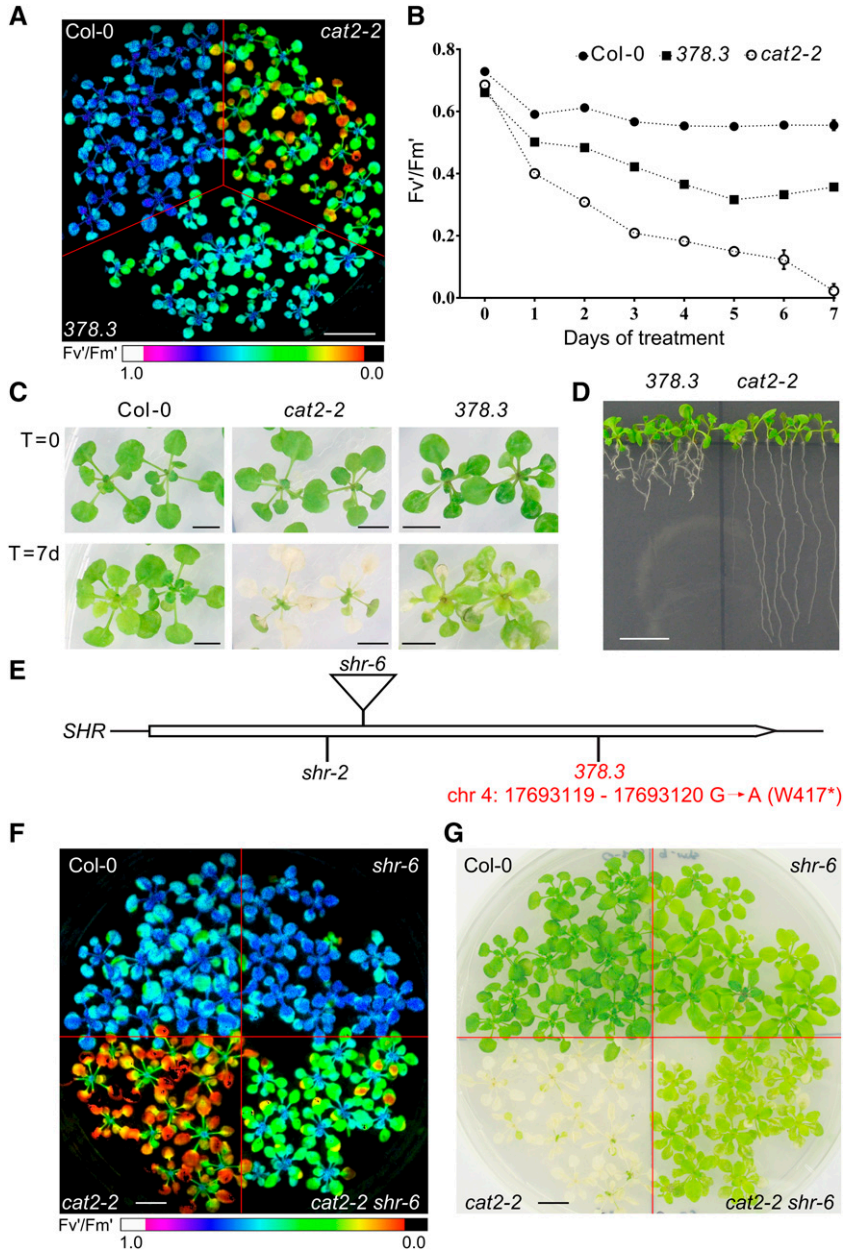

Figure 2. Characterization of Line *378.3*.

(A) Color-coded images of PSII maximum efficiency (F_v'/F_m') of 3-week-old Col-0, *378.3*, and *cat2-2* plants exposed to photorespiration-promoting conditions (restricted gas exchange and transfer to continuous light) for 24 h. Bar = 20 mm.

(B) F_v'/F_m' decrease during the exposure to photorespiration-promoting conditions in Col-0, *378.3*, and *cat2-2* plants. Data points represent means of three biological replicates ±SE.

(C) Representative bright-field images of Col-0, *cat2-2*, and *378.3* before (top) and after (bottom) 7 d of exposure to photorespiration-promoting conditions. Bar = 5 mm.

(D) Short-root phenotype of *378.3*. Plants were grown vertically for 2 weeks on MS medium supplemented with 1% (w/v) sucrose under long-day (LD) conditions (16 h/8 h day/night) at 100 μmol m^{-2} s^{-1}. Bar = 10 mm.

(E) Gene model of *SHR* with positions of mutant alleles used in this study. The identified mutation site is marked in red.

(F) Color-coded F_v'/F_m' images of 3-week-old Col-0, *cat2-2*, *shr-6*, and *cat2-2 shr-6* plants exposed to photorespiration-promoting conditions for 48 h. Colors are as in Figure 1A. Bar = 10 mm.

(G) Representative bright-field image of 3-week-old Col-0, *cat2-2*, *shr-6*, and *cat2-2 shr-6* plants after 7 d of exposure to photorespiration-promoting conditions. Bar = 10 mm.

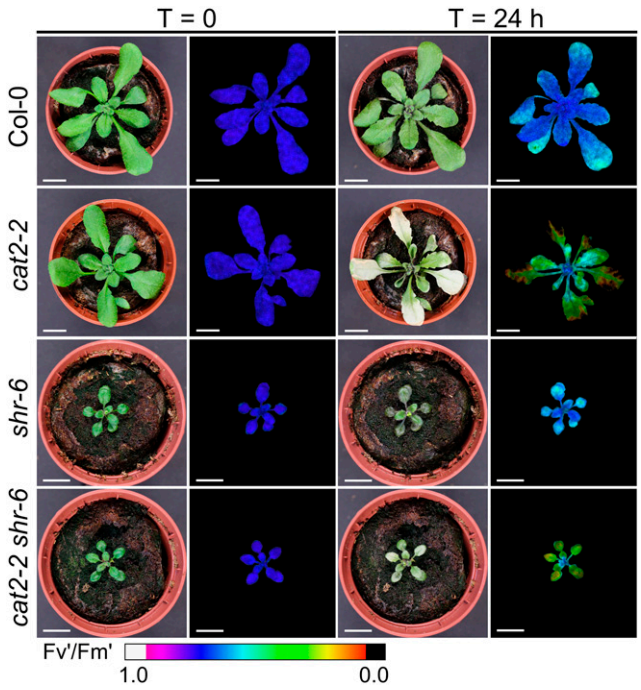

Figure 3. Effect of SHR Deficiency on the Photorespiratory Phenotype of *cat2-2* in Soil Conditions.

Three-week-old plants grown in a high CO_2 (3000 μL L^{-1}) atmosphere at 100 μmol m^{-2} s^{-1} were transferred to ambient air and exposed to continuous high light (1000 μmol m^{-2} s^{-1}). Pairs of images show representative bright-field images (left panels) of 3-week-old plants, together with color-coded F_v'/F_m' images (right panels) in the beginning (t = 0) and 24 h after the onset of the exposure to photorespiration-promoting conditions (t = 24 h). Colors are as in Figure 1A. Bar = 10 mm.

a higher AA content than that of the wild type both under control and stress conditions (Figure 5A). We identified ~300 ROS-responsive transcripts (Supplemental Data Set 2) from a compendium of five microarray experiments featuring ROS-generating conditions and assessed their expression levels upon exposure to photorespiration-promoting conditions in the different mutant genotypes (Figure 5B). The induction of the ROS-responsive transcripts was especially pronounced in *cat2-2* mutants, whereas their induction was alleviated in *shr-6 cat2-2* mutants. Interestingly, the expression levels of most ROS-responsive transcripts were not affected in *shr-6* single mutants exposed to photorespiration-promoting conditions (Figure 5B). Taken together, our data indicate that SHR loss of function leads to a more reduced cellular redox environment pointing toward decreased H_2O_2 levels.

Lack of SHR Negatively Affects Photosynthetic CO_2 Assimilation and Photorespiratory Metabolism

GOX activity in photosynthesizing tissues generates substantial amounts of H_2O_2 that are subsequently removed by peroxisomal CAT. To test whether aberrant GOX and CAT activities might explain the more reduced redox environment in the absence of SHR, we measured their activities in *shr-6* leaf extracts under control conditions. Plants lacking SHR displayed significantly lower GOX (47%) and CAT (61%) activities than did the wild type (Figure 6A). The impaired GOX activity in control *shr-6* plants did not correlate with reduced transcript abundancies of the two photorespiratory *GOX* isoforms *GOX1* and *GOX2*, whereas *CAT2* mRNA levels were slightly lower than those of the wild type (log_2 fold change = −0.58; P = 0.06; Supplemental Data Set 3).

Photorespiration and photosynthesis are intimately linked and enhanced rates of CO_2 assimilation are accompanied by increased flux via the photorespiratory pathway (Peterhansel and Maurino, 2011). On the other hand, blockage of the photorespiratory pathway leads to inhibition of photosynthesis (Peterhansel and Maurino, 2011). To estimate whether low activities of GOX and CAT impact CO_2 assimilation, in vitro-grown *shr-6*, *cat2-2 shr-6*, *cat2-2*, and wild-type plants were compared. The photosynthetic rates of *shr-6* and *cat2-2 shr-6* mutants were significantly lower (37 and 53%) than the corresponding controls (Figure 6B).

The reduced CO_2 assimilation and lowered GOX and CAT enzyme activities implied that the photorespiratory pathway in *shr-6* mutants might be impaired. To further test this hypothesis, we quantified the steady state levels of selected photorespiratory intermediates under control and photorespiratory conditions. The reduced CO_2 assimilation observed in *shr-6* and *cat2-2 shr-6* mutants before exposure to photorespiratory conditions was accompanied by elevated levels of glycolate that were especially pronounced in the double mutant (Figure 6C). Exposure to photorespiration-promoting conditions increased glycolate content to comparable levels in *cat2-2* and *shr-6*, whereas in *cat2-2 shr-6* double mutants, the glycolate amounts were ~70-fold higher than in wild-type plants (Figure 6C). By contrast, the glycine content of *shr-6* and *cat2-2 shr-6* mutants was lower than that in wild-type and *cat2-2* plants under control conditions (Figure 6C). During the treatment, only wild-type plants accumulated glycine (Figure 6C). Serine pools were largely unaffected by the enhanced rates of photorespiration in all genotypes, but *cat2-2* and *cat2-2 shr-6* mutants displayed elevated serine contents, regardless of the treatment (Figure 6C). Taken together, these results hint at a blockage of the photorespiratory pathway in *shr* mutants upstream of glyoxylate transamination.

Loss of SHR Does Not Affect Peroxisome Biogenesis

Accumulation of glycolate, low abundance of downstream photorespiratory metabolites (Figure 6C), and the partial requirement for exogenous sucrose to support postembryonic growth (Supplemental Figure 4; Cui et al., 2012) suggested that *shr* mutants might be deficient in peroxisome development. Germination of most peroxisome biogenesis mutants (*pex*) (Nito et al., 2007) is insensitive to indole-3-butyric acid and 2,4-dichlorophenoxybutyric acid because their conversion to the biologically active metabolites indole-3-acetic acid and 2,4-D, respectively, requires glyoxysomal/peroxisomal β-oxidation (Hayashi et al., 1998; Zolman and Bartel, 2004). Therefore, *shr-6* seedlings were germinated on media supplemented with 10 μM indole-3-butyric acid or 0.2 mg mL^{-1} 2,4-dichlorophenoxybutyric acid, but no differences to the wild type were observed.

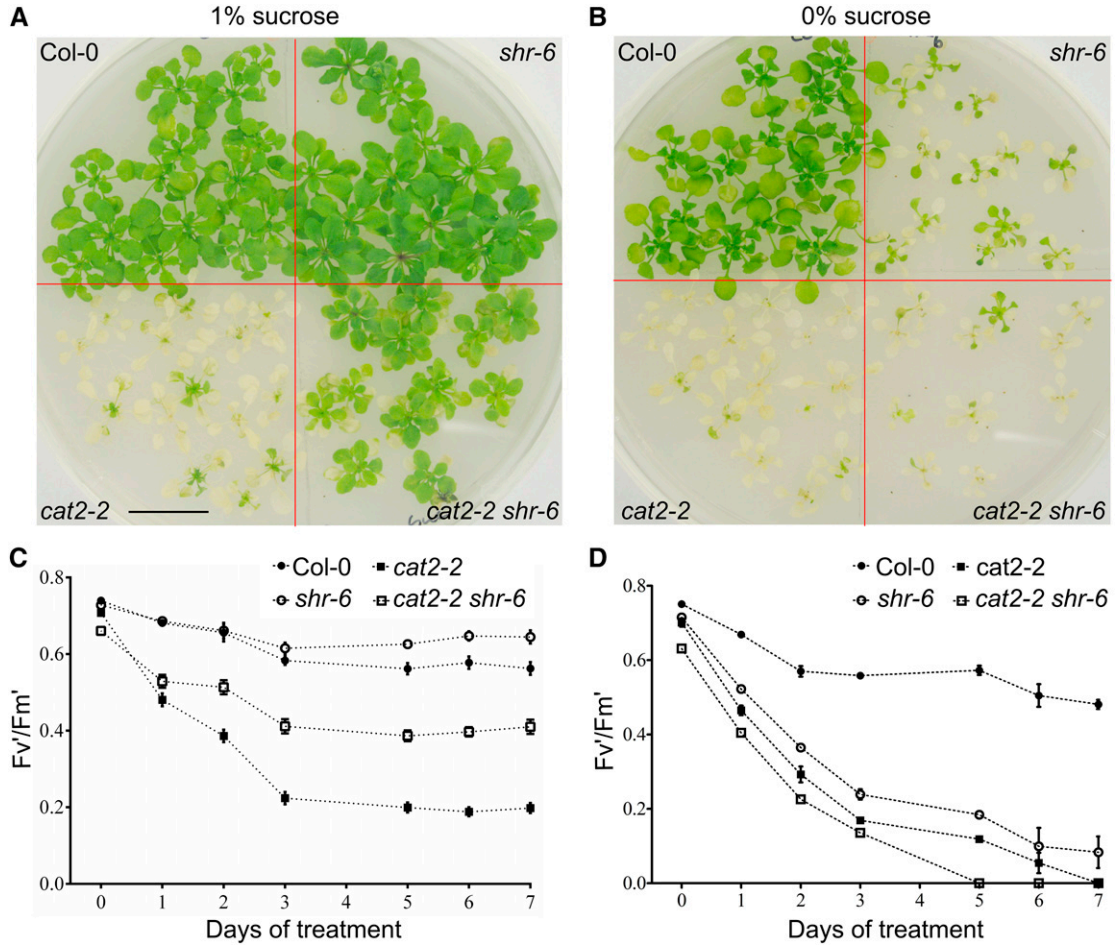

Figure 4. Influence of Exogenous Sucrose on the Tolerance of SHR-Deficient Plants to the Photorespiration-Promoting Conditions.

Plants were germinated and grown for 18 d on a nylon mesh placed on a 1× MS sucrose-supplemented medium (1% w/v) and subsequently transferred either to a medium with a similar sucrose concentration or to a sucrose-free medium. Three days after the transfer, plants were exposed to photorespiration-promoting conditions.

(A) and **(B)** Representative bright-field images of plants exposed to photorespiration-promoting conditions for 7 d on medium containing 1% (w/v) sucrose **(A)** and on medium with no sucrose **(B)**. Bar = 20 mm.

(C) and **(D)** Photorespiration-triggered F_v'/F_m' changes over time in Col-0 (closed circles), *cat2-2* (closed squares), *shr-6* (open circles), and *cat2-2 shr-6* (open squares) plants. Data points represent means of three biological replicates ±SE.

Additionally, we introduced the peroxisomal marker *Pro35S:PTS1:GFP* (Zolman and Bartel, 2004) into the *shr-6* background and investigated peroxisomal numbers and dynamics, but again could not detect differences in comparison to the wild type (Supplemental Figure 5).

Lack of SCR Does Not Alleviate the Cell Death Phenotype of *cat2-2* Mutants under Photorespiration-Promoting Conditions

The SHR-SCR complex positively regulates the expression of SCR by binding to its promoter. As a result, both *shr* and *scr* mutants display similar molecular and phenotypic characteristics (Cui et al., 2007). Surprisingly, the introduction of the *scr-3* allele into *cat2-2* background not only did not alleviate the photorespiratory phenotype in the absence of peroxisomal catalase but also rendered the *cat2-2 scr-3* double mutants more susceptible to photorespiration-promoting conditions (Figures 7A and 7B). Moreover, two independent *scr* knockout alleles, *scr-3* and *scr-1*, displayed a lower stress tolerance than the respective wild-type controls (Figures 7C and 7D). Taken together, these results indicate that SHR acts independently of SCR in modulating stress responses under photorespiration-promoting conditions. Additionally, because the *cat2-2 scr-3* mutants similarly exhibit a short root phenotype, these results also provide evidence that the impaired root growth by itself is not responsible for the survival phenotype.

Mutants lacking SHR and SCR exhibit a number of overlapping sugar-related phenotypes, such as sugar-sensitive germination, inability to mobilize starch, and increased levels of glucose,

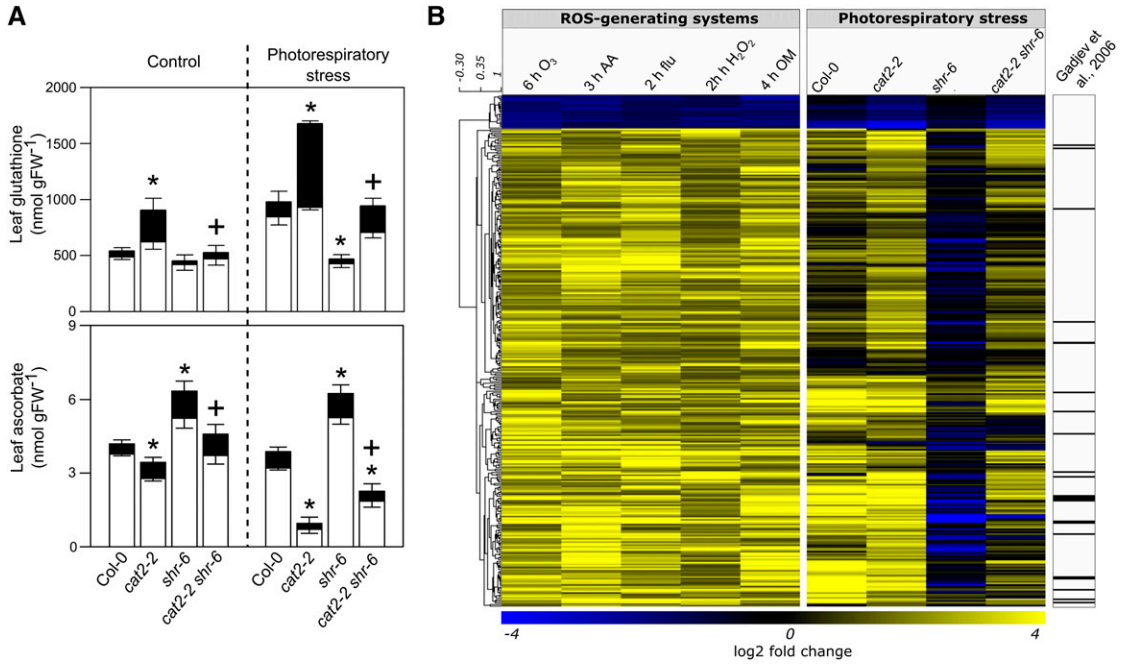

Figure 5. Cellular Redox Alterations in the Absence of Functional SHR.

(A) Glutathione and ascorbate content in 3-week-old Col-0, *cat-2*, *shr-6*, and *cat2-2 shr-6* plants before (Control) and after (Photorespiratory stress) 24 h of exposure to photorespiration-promoting conditions. White bars indicate GSH or AA content, and black bars indicate GSSG or dehydroascorbate (DHA) content averaged from four biological replicates ±SE. Asterisk indicates significant difference of all mutant genotypes relative to Col-0 at $P < 0.05$, and + indicates significant difference between *cat2-2* and *cat2-2 shr-6* at $P < 0.05$ for total glutathione (GSH + GSSG) and ascorbate (AA + DHA).

(B) Comparison of expression patterns of a subset of ROS-responsive genes that are found in the transcriptome signatures of Col-0, *cat2-2*, *shr-6*, and *cat2-2 shr-6* plants upon exposure to photorespiration-promoting conditions. The following experiments were used in the analysis: exposure of seedlings to ozone for 6 h (6 h O_3, E-MEXP-342); treatment of seedlings with 50 μM antimycin A for 3 h (3 h AA, GSE41136); reillumination of the conditional *flu* mutant for 2 h after a dark acclimation (2 h *flu*, GSE10812); treatment of seedlings with 10 mM H_2O_2 for 24 h (24 h H_2O_2, unpublished data), and treatment of seedlings with oligomycin for 4 h (4 h OM, GSE38965). ROS marker genes published previously (Gadjev et al., 2006) are shown alongside the heat map.

fructose, and sucrose (Cui et al., 2012, 2014). However, a notable difference between the two mutants is the transcript abundance of the important mediator of sugar signaling ABSCISIC ACID INSENSITIVE4 (ABI4). Interestingly, ABI4 transcripts are strongly induced in *scr* but not in *shr* mutants. Therefore, we investigated whether the high ABI4 levels might be responsible for the differential responses of *cat2-2 scr-3* and *cat2-2 shr-6* under photorespiration-promoting conditions in the presence of sugars. To test this hypothesis, we introduced the *abi4-102* mutation (Laby et al., 2000) into the *cat2-2* background and exposed the resulting *cat2-2 abi4-102* double mutants to photorespiration-promoting conditions in vitro. Despite the lack of ABI4, *cat2-2 abi4-102* mutants were indistinguishable from the parental *cat2-2* plants in terms of F_v'/F_m' decrease and timing of lesion formation (Supplemental Figure 6).

DISCUSSION

In Arabidopsis *cat2* mutants, H_2O_2 production can be efficiently modulated through changes in CO_2 partial pressure and light intensity (Vanderauwera et al., 2005; Queval et al., 2007; Kerchev et al., 2015). Decreased levels of CO_2 favor the Rubisco oxygenation reaction and lead to an increased flux via the photorespiratory pathway (Laing et al., 1974). As an experimental approach to conditionally modulate photorespiration and associated H_2O_2 production in Arabidopsis seedlings, we depleted the CO_2 levels by restricting the gas exchange of the Petri dishes by sealing them with Parafilm and forcing the plants to perform full-time photosynthesis by continuous growth in the light (Kerchev et al., 2015). These conditions trigger a rapid and homogenous decrease in CO_2 levels within the growth environment and thereby enhance the flux via the photorespiratory pathway, as clearly evidenced by both the altered levels of photorespiratory metabolites and the cell death phenotype observed in *cat2-2* mutants (Figure 1; Kerchev et al., 2015). A conceptually similar system for experimental decrease in CO_2 levels to screen for photorespiratory mutants in air-tight chambers had already been proposed to screen soybean (*Glycine max*) plants for individuals with reduced photorespiratory rates (Widholm and Ogren, 1969).

In a seminal forward genetics screen that identified the first photorespiratory mutants in Arabidopsis, photorespiration had been imposed by growing plants first under a CO_2-enriched atmosphere (1% CO_2/21% O_2) before shifting them to ambient air (Somerville and Ogren, 1979). Alternatively, leaf gas exchange was restricted by sealing stomata with lanolin. The enforced drop in the stomatal conductance swiftly provoked increased

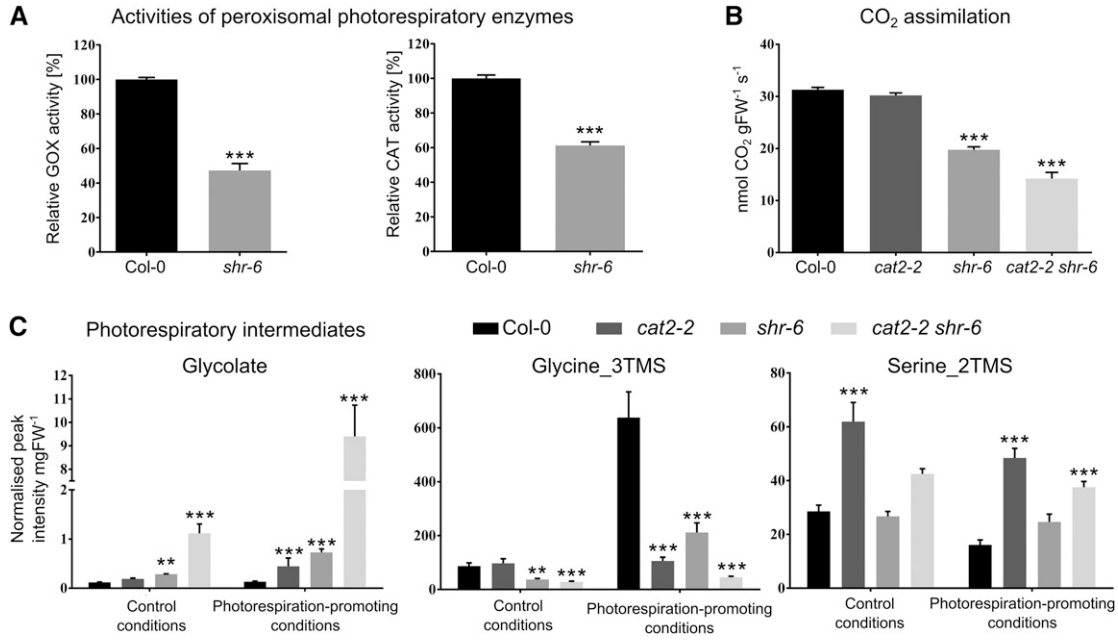

Figure 6. Effect of SHR Deficiency on Photosynthetic CO_2 Assimilation and Photorespiratory Metabolism.

(A) Impact of SHR deficiency on the activities of the peroxisomal photorespiratory enzymes glycolate oxidase and catalase. Enzyme activities were extracted from 2-week-old rosettes of Col-0 and *shr-6* plants and are expressed as a percentage of Col-0 values. Bars represent means of three biological replicates ±SE. Asterisks (*P < 0.05, **P < 0.01, and ***P < 0.001) indicate significance according to Student's *t* test.

(B) CO_2 assimilation of 3-week-old in vitro-grown Col-0, *cat2-2*, *shr-6*, and *cat2-2 shr-6* plants. Values represent means of eight biological replicates ±SE. Asterisks (*P < 0.05, **P < 0.01, and ***P < 0.001) show significant differences relative to Col-0 identified by a one-way ANOVA followed by Dunnett's multiple comparisons post hoc test.

(C) Levels of glycolate, glycine, and serine under control and photorespiration-promoting conditions (24 h) in 3-week-old in vitro-grown plants. Glycine and serine levels were quantified based on the abundance of 3-trimethylsilyl (TMS) and 2-TMS derivatives, respectively. Values represent means of five biological replicates ±SE. Data were analyzed with a two-way ANOVA with treatment (photorespiration-promoting conditions versus control conditions) and genotype as main factors, followed by a Tukey's multiple comparison post hoc test. Asterisks (*P < 0.05, **P < 0.01, and ***P < 0.001) show significant differences to Col-0 within the respective conditions.

photorespiration and H_2O_2 accumulation (Mateo et al., 2004). In comparison to these approaches, the main advantage of our experimental system is the possibility of screening plants in a high-throughput manner, with a reduced risk for false positives. Control of the atmospheric CO_2/O_2 concentration ratio requires specialized growth chambers, additionally limiting throughput and, hence, the feasibility of the assay on a wider scale. In previous attempts to perform a similar screen in soil-grown plants, we failed to identify mutant plants with reproducible phenotypes. In the current assay, we screened more than 100,000 M2 plants. The high-throughput characteristics of the assay were additionally favored by the noninvasive chlorophyll fluorescence readout, making this in vitro bioassay an excellent choice for large-scale screening and follow-up experiments. The decrease in the treatment-associated PSII efficiency occurs before the visible cell death lesions and therefore serves as an early proxy for stress symptoms (Figure 1). A limitation of the assay is its in vitro setup and the presence of sugar in the growth medium that unavoidably influences photosynthesis, development, and stress responses. However, *cat2* and other photorespiratory mutants require exogenous sugar supplementation for proper growth in vitro (Timm and Bauwe, 2013). Therefore, the screen was conducted with the use of sucrose-supplemented growth medium that together with the potential accumulation of volatile metabolites, such as ethylene and methyl jasmonate, might influence the stress responses.

Here, we report the identification of a causative mutation in the SHR transcription factor that enables survival of *cat2-2* mutants under photorespiratory conditions and dissect the physiological, biochemical, and transcriptomic changes that underlie this process. Several lines of evidence support a scenario under which *SHR* loss-of-function attenuates the impact of exposure to photorespiration-promoting conditions, largely through reduced H_2O_2 accumulation. In support, *shr-6* and *cat2-2 shr-6* mutants accumulate enhanced levels of ascorbate under control conditions in comparison to the wild type and single *cat2-2* mutants, respectively, and the decrease in ascorbate levels observed under photorespiration-promoting conditions in *cat2-2* is attenuated in the double mutants (Figure 5A). Second, the glutathione accumulation in *cat2-2 shr-6* mutants under stress conditions is largely abolished when compared with that of the *cat2-2* mutants, and its redox status is not affected by the treatment (Figure 5A). Third, the ROS transcriptome signature of *cat2-2 shr-6* under photorespiration-promoting conditions resembles that of the wild type rather than that of the parental *cat2-2* and the accumulation

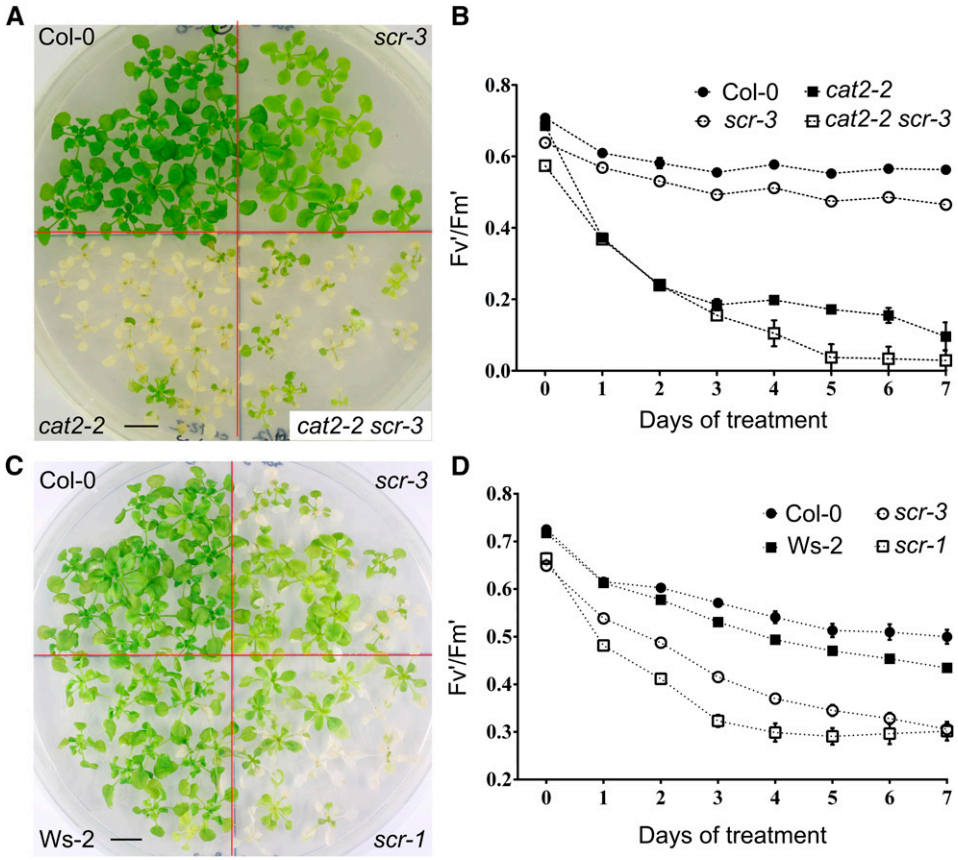

Figure 7. Influence of SCR on the Photorespiratory Phenotype of *cat2-2*.

(A) and **(B)** The photorespiratory phenotypes of *cat2-2* and *cat2-2 scr-3*. Representative bright-field images illustrating cell death lesion formation in *cat2-2* and *cat2-2 scr-3* plants 1 week following the onset of exposure to photorespiration-promoting conditions **(A)**, together with changes of F_v'/F_m' over time **(B)**. Data points represent means of three biological replicates ±SE. Bar = 10 mm.

(C) and **(D)** Performance of independent *scr* alleles (*scr-3* and *scr-1*) during exposure to photorespiration-promoting conditions. Representative bright-field images illustrating cell death lesion formation in *cat2-2* and *cat2-2 scr-3* plants 1 week after the onset of treatment **(C)**, together with changes of F_v'/F_m' over time **(D)**. Data points represent means of three biological replicates ±SE. Bar = 10 mm.

of ROS-induced transcripts in single *shr-6* mutants is virtually absent (Figure 5B). Finally, in the *shr-6* mutant, the photosynthetic CO_2 assimilation was lower than that of wild-type and *cat2-2* plants and was accompanied by reduced GOX and CAT activities (Figure 6). Glycolate accumulation in *shr-6* mutants, jointly with decreased GOX activities and impaired photosynthesis, implies that the flux through the photorespiratory pathway, and, hence, peroxisomal H_2O_2 production, are reduced in mutants carrying *shr-6*. Therefore, this partially restricted photorespiratory activity conferred by *shr-6* might be sufficient to attenuate the cell death of *cat2-2* mutants under in vitro photorespiration-promoting conditions but not to counteract the effects in soil-grown plants after transfer to high light intensities of 1000 μmol m^{-2} s^{-1} (Figure 3).

Comparison of the transcriptomes under control conditions revealed similarities between *shr-6* and *cat2-2* single mutants (Supplemental Figure 7). Under these conditions, the redox status of *cat2-2* is already perturbed, as also evidenced by the increased levels and oxidation status of glutathione and the constitutive expression of numerous ROS-related transcripts. The redox perturbation of *cat2-2* has been shown to involve accumulation of SA and pathogenesis-related transcripts (Chaouch et al., 2010; Li et al., 2014). The activation of such responses in the *cat2-2* background has been largely attributed to the oxidized environment and accumulation of H_2O_2 (Chaouch et al., 2010). Among the transcripts induced in *shr-6* were the SA marker gene *PR-1* and numerous ROS-related genes, suggesting that *shr-6* mutants are in a primed state that underlies their subsequent response to photorespiration-promoting conditions. In contrast to *cat2-2*, however, the glutathione levels and its oxidation status in *shr-6* were similar to those of the wild type; more importantly, they accumulated ascorbic acid, suggesting that the redox homeostasis is tightly regulated. The elevated ascorbate content was accompanied by increased transcript levels of several ascorbate biosynthetic genes from the L-galactose pathway (Supplemental Figure 8). Ascorbate-deficient mutants have been shown to accumulate SA via yet unidentified mechanisms, implying a link between pathogen responses and ascorbate levels (Mukherjee et al., 2010). Despite the available literature describing activation

of SA signaling in mutants with low ascorbate levels, the intimate link between ascorbate levels and SA accumulation cannot exclude the opposite scenario under which high ascorbate triggers SA synthesis. Mutants carrying the *shr-6* mutation also displayed enhanced myo-inositol levels (Supplemental Figure 9) together with increased transcript abundance of two myo-inositol oxygenase-encoding genes, *MIOX2* and *MIOX4* (Supplemental Data Set 1). Myo-inositol might be functionally linked to ascorbic acid biosynthesis, although the exact contribution of these steps is far from elucidated (Lorence at al., 2004; Endres and Tenhaken, 2009). Besides its potential role in ascorbic acid biosynthesis, myo-inositol has been shown to negatively regulate cell death and supplementing *cat2-2* mutants with exogenous myo-inositol can attenuate photorespiratory-dependent cell death (Chaouch and Noctor, 2010). Interestingly, *myo-inositol-1-phosphate synthase1* mutants deficient in the enzyme catalyzing the rate-limiting step of myo-inositol synthesis display light-dependent lesion formation in a SA-dependent manner similarly to *cat2-2* mutants (Donahue et al., 2010).

Among the target genes of SCR and SHR are numerous stress-associated genes. This knowledge has led to the hypothesis that these transcription factors play a dual role in plant growth and development (Cui et al., 2011). Despite their hypersensitivity to abscisic acid, however, both *shr* and *scr* display wild-type sensitivity to mannitol and salinity (Cui et al., 2012). We have similarly examined the growth characteristics of *shr-6* to two different concentrations of mannitol (25 and 50 mM) and salt (50 and 100 mM) and did not observe any differences in their response relative to the wild type (Supplemental Figures 10A and 10B). As the primary cause for the cell death phenotype of *cat2-2* is H_2O_2 accumulation, we tested how *shr-6* mutants react to exogenous H_2O_2 and found that the response was comparable to that of the wild type (Supplemental Figure 10C). Because the primary mechanism that leads to attenuation of the cell death phenotype of *cat2-2* is the limited flux via the photorespiratory pathway in combination with priming of the stress response, it is not surprising that other stress treatments cannot be alleviated in the absence of SHR. However, the constitutive expression of ROS-related transcripts, enhanced ascorbate content, and effects on photosynthesis further strengthen the role of SHR as a modulator of stress responses.

Despite the agonistic involvement of SHR and SCR in root growth and development and the overlapping transcriptome signatures of the two mutants, certain genotype-specific functions can be deconvoluted by examining their expression patterns and mutant phenotypes. *SCR* transcript abundance is largely governed by the presence of *SHR*, but reduced *SCR* levels can also be found in a *shr* background, implying the existence of SHR-independent mechanisms of *SCR* expression (Dhondt et al., 2010). The differential role of SHR and SCR in attenuating the cell death phenotype of *cat2* might be clarified by the target genes that are not common between the two transcription factors. For example, among the unique SHR targets are two transcription factors NUTCRACKER (At5g44160) and BASIC LEUCINE-ZIPPER2 (At2g18160; Cui et al., 2011). Interestingly, both of them are phosphorylated by KIN10 that is often described as a master regulator of plant metabolism on which developmental, stress, and sugar signals converge (Baena-González et al., 2007).

Future efforts are needed to gain insights into the mechanistic events underlying the phenotypes presented in this work. SHR had already been demonstrated to bind to the promoters of a wide variety of genes that function in diverse cellular processes (Cui et al., 2007, 2011, 2014). Therefore, future research should focus on a comprehensive functional analysis of downstream SHR targets with the aim of identifying the genetic interaction network that is responsible for the described photorespiratory phenotypes. Initially, we demonstrated that SHR affects the photorespiratory pathway independently from SCR (Figure 7). With the largely overlapping shoot transcriptomes of *shr* and *scr* (Dhondt et al., 2010), target genes that are differentially regulated by SHR and SCR, respectively, could be prioritized. At the time of the photorespiratory treatment, *SHR* expression in the leaf is restricted to the vascular tissues (Cui et al., 2014). Interestingly, within leaf tissues, SHR migrates to the adjacent cell layers (Gardiner et al., 2010) as observed similarly in roots (Nakajima et al., 2001; Cui et al., 2007). SHR exerts its molecular function largely through protein-protein interactions (Cui et al., 2007; Welch et al., 2007), but the composition of the shoot SHR interactome is still unknown. We anticipate that efforts aiming at investigating the shoot SHR-interacting proteins will provide a better understanding of the SHR function in the leaf.

In conclusion, our results reveal an unanticipated role of SHR in the control of cellular redox homeostasis and photorespiratory metabolism. The absence of SHR attenuated the photorespiration-induced cell death in plants lacking CAT2 in a SCR-independent manner. Lack of functional SHR had a marked effect on the cellular redox homeostasis that, together with perturbed photorespiratory metabolism and attenuated induction of ROS-responsive transcripts, indicated a reduced photorespiratory H_2O_2 accumulation. These findings strengthen the link between plant development and oxidative stress responses and provide direction for further investigations of a tight interplay between these processes.

METHODS

Plant Material

The mutant lines used in this study have been described previously: *cat2-2* (Queval et al., 2007), *shr-6* (Dhondt et al., 2010; Yu et al., 2010), *shr-2* (Fukaki et al., 1998), *scr-1* (Di Laurenzio et al., 1996), *scr-3* (Fukaki et al., 1996), and *abi4-102* (Laby et al., 2000). Line ET8347 (*cat2-20*) was obtained from the Cold Spring Harbor Laboratory TRAPPER collection (http://genetrap.cshl.edu; Sundaresan et al., 1995). Plants homozygous for the DsE insertion were selected by PCR and the DsE-gene junctions were sequenced with primers used for their amplification (Supplemental Table 1) to map the insertion site. The double knockout lines *cat2-2 scr-3*, *cat2-2 shr-6*, and *cat2-2 abi4-102* were generated by crossing *cat2-2* plants (pollen acceptors) with the respective mutant lines (pollen donors). Double mutant plants were identified in F2-segregating populations by both root length phenotype and PCR/derived cleaved amplified polymorphic sequences (dCAPS) genotyping with the respective primers/restriction enzymes (Supplemental Table 1). dCAPS markers were designed with dCAPS Finder 2.0 (Neff et al., 2002). To obtain F1 individuals heterozygous for the *SHR* locus in the Col-0 and *cat2-2* background, *shr-6* mutants were crossed with Col-0 plants and the *cat2-2 shr-6* double mutant line was crossed with *cat2-2* plants. For the investigation of peroxisomal behavior, the transgenic *Pro35S:PTS1:GFP* line (Zolman and Bartel, 2004) was crossed with the *shr-6* mutant. The F2-segregating population was examined for root length phenotype and GFP signal to identify GFP-positive *shr-6* plants.

Mutagenesis and Screening for Revertants of the *cat2-2* Photorespiratory Phenotype

Seeds of the *cat2-2* T-DNA mutant line (Queval et al., 2007) were treated with a 0.3% (w/v) EMS solution for 7.5 h, washed extensively with water, and sown in vinyl pots. M1 plants were grown at 21°C under a short-day regime (8 h light [100 μmol m^{-2} s^{-1}]/16 h dark). Before M2 seeds were harvested, the number of M1 plants in each pot was counted. Recessive mutants segregated in a 7:1 ratio in an M2 population; therefore, 10 M2 plants per M1 plant were analyzed. Mutagenized M2 plants were grown in Petri dishes (150 × 25 mm; Becton-Dickinson) on full-strength MS agar-solidified medium supplemented with 1% (w/v) sucrose, 100 mg L^{-1} myo-inositol, 0.5 mg L^{-1} nicotinic acid, 0.5 mg L^{-1} pyridoxine, and 1 mg L^{-1} thiamine at 21°C and long-day (LD) conditions (16 h light [100 μmol m^{-2} s^{-1}]/8 h dark). Each plate contained ~60 M2 plants and six wild-type (Col-0) seedlings. To promote photorespiration, after 21 d of growth, the Micropore surgical tape (3M) that sealed the plates was replaced by two layers of Parafilm M (Bemis) to restrict gas exchange. Plants were transferred to continuous light. Changes in maximum efficiency of the PSII photochemistry (F_v'/F_m') were determined with an Imaging PAMM-series (MAXI version) chlorophyll fluorometer and ImagingWin software (Heinz Walz). The F_v'/F_m' parameter was visualized spatially with ImagingWin software that uses a false color scale ranging from black ($F_v'/F_m' = 0.0$) to white ($F_v'/F_m' = 1.0$) with red, orange, yellow, blue, violet, and purple in between. The putative mutants that showed a reduced lesion formation and decreased F_v'/F_m' ratio were transplanted to soil to obtain M3 seeds. The M3 plants were retested with the same experimental conditions to determine whether they exhibited the parental phenotype. Confirmed mutants were selected to produce M4 seeds.

Mapping Strategy

To identify the causative mutation, *Arabidopsis thaliana* plants, accession Landsberg *erecta* (L*er*-0), that lack peroxisomal catalase (*cat2-20*) were identified and confirmed genetically and biochemically (Supplemental Figure 11). Subsequently, *cat2-20* plants were crossed with the *378.3* mutant. Approximately 25% of the F2 plants exhibited a delay in the onset of cell death, indicating that the trait is determined by a single recessive mutation.

In parallel, we examined the *378.3* inventory of EMS-induced polymorphisms (G→A and C→T) by next-generation sequencing (see below; Supplemental Data Set 4) to identify mutations responsible for the observed phenotype. A mutation introducing the premature stop codon (4:17693120 G→A, W417*) in the coding sequence of the SHR transcription factor was selected as the most prominent candidate (Figure 2E; Supplemental Data Set 4) because within the F2 population, the improved survival under photorespiration-promoting conditions perfectly cosegregated with reduced root length (Figure 2D), stunted growth, and increased anthocyanin content, all of which are characteristics of SHR-lacking plants (Benfey et al., 1993; Scheres et al., 1995; Dhondt et al., 2010). Moreover, as demonstrated by genotyping with a dCAPS marker, all F2 plants (177 individuals) that exhibited a delay in the onset of cell death had the premature stop codon (see above).

Production of Anti-CAT2 Rabbit Polyclonal Antibodies

The *CAT2*-coding sequence was amplified from Arabidopsis Col-0 cDNA with Phusion High-Fidelity DNA Polymerase (Thermo Fisher Scientific) with primers cat2_F_attB1 and cat2_R_attB2 (Supplemental Table 1) according to the manufacturer's instructions. The PCR product was cloned by recombination into the pDONR221 plasmid (Invitrogen). After sequence verification, the coding sequence was subcloned into the pDEST17 expression vector (Invitrogen) and then transformed into *Escherichia coli* BL21(DE3)pLysS strain for expression. A 5-mL volume of Luria-Bertani Miller broth (1% [w/v] peptone, 0.5% [w/v] yeast extract, and 1% [w/v] NaCl) supplemented with 100 mg mL^{-1} ampicillin and 25 mg mL^{-1} chloramphenicol was inoculated and grown overnight at 37°C with agitation at 220 rpm. This culture was diluted to 500 mL, grown for 2 h at 37°C and at 220 rpm, and induced with 0.2 mM isopropyl β-D-1-thiogalactopyranoside. After 24 h of induction at 20°C and at 220 rpm, cells were harvested by centrifugation at 4,000*g* for 10 min and resuspended in 100 mL of lysis buffer (20 mM AMPSO, pH 8.5, 0.3 M NaCl, 1 mM PMSF, and 2 units mL^{-1} DNase I). Bacterial cells were disrupted by sonication and centrifuged at 16,100*g* for 20 min at 4°C. The insoluble protein fraction was denatured at 96°C in loading buffer supplemented with 5 mM β-mercaptoethanol and examined by SDS-PAGE. The protein band corresponding to CAT2 was excised from gel and submitted for generation of polyclonal rabbit antibodies (Eurogentec).

Enzyme Activity Measurements and Immunoblot Analysis

For catalase activity measurements, tissue was ground with a MM 400 ball mill (Retsch) and mixed with extraction buffer (60 mM Tris-HCl, pH 6.9, 10 mM DTT, 20% [v/v] glycerol, and 1 mM PMSF) at a 1:1 ratio (v/v). The homogenate was centrifuged at 16,100*g* for 15 min at 4°C. The supernatant was used in a spectrophotometric catalase activity assay (Clare et al., 1984) and for SDS-PAGE protein separation.

For immunoblot analysis, 10 μg of leaf protein was separated on a 12.5% SDS-PAGE gel, blotted onto a polyvinylidene fluoride membrane (Millipore), and hybridized with a 1:3500 dilution of rabbit antiserum against Arabidopsis CAT2 developed herein.

Glycolate oxidase activity was measured as described (Rojas et al., 2012), with a protocol downscaled for 200 mg of ground tissue. Briefly, shoot tissue was collected, frozen in liquid nitrogen, and ground with a MM 400 ball mill (Retsch). This material was mixed with 1 mL of extraction buffer by vortexing and centrifuged at 16,100*g* for 30 min at 4°C. The protein concentration in the soluble phase was determined with the Bradford Assay (Bio-Rad). Next, 10 μL of supernatant was used in a spectrophotometric glycolate oxidase activity assay conducted in a VersaMax microplate reader (Molecular Devices) at room temperature for 1 h. The glycolate oxidase activity was measured by monitoring the H_2O_2-dependent oxidation of *O*-dianisidine into a colored *O*-dianisidine radical cation by following the associated absorption increase at 440 nm. The specific activity was calculated by dividing the change in absorbance (ΔA) by the time and the amount of soluble protein present in the sample (ΔA min^{-1} mg^{-1}) and was then expressed as a percentage of control. All enzymatic assays were done on three biological replicates with at least three technical repeats.

Real-Time PCR

For the quantification of transcript levels, total RNA was prepared with the RNeasy Plant Mini Kit (Qiagen). First-strand cDNA was synthesized with the iScript cDNA Synthesis Kit (Bio-Rad) with 1 μg of total RNA used as input material. Five microliters of the 1:8 diluted first-strand cDNA was used as a template in the subsequent PCR run on the iCycler iQ (Bio-Rad) with gene-specific primers (Supplemental Table 1). Reactions were done in three technical repeats with the SYBR Green I Master kit (Roche), according to the manufacturer's instructions. Transcript abundance was quantified with the qBASEPlus software (Biogazelle) using *ACTIN-RELATED PROTEIN7* and *SERINE/THREONINE PROTEIN PHOSPHATASE2A* (*PP2A*) as reference genes (unless specified otherwise). All experiments were done with three biological replicates.

Next-Generation Sequencing

For the identification of the EMS-induced mutations in the *378.3* mutant, M3 plants were grown for 21 d under LD conditions on agar-solidified MS medium supplemented with 1% (w/v) sucrose. Bulked shoot tissue was

ground in liquid nitrogen and 2 g of powder was used as the starting material for nuclear DNA extraction as described previously (Schneeberger et al., 2009). Enrichment of nuclear DNA was confirmed by a quantitative PCR analysis with the described primers (Schneeberger et al., 2009).

Library preparation, sequencing, and annotation of single nucleotide polymorphism/insertion-deletions (SNP/InDels) were performed by Fasteris. Paired-end libraries were sequenced with an Illumina Hi-Seq 2000 sequencing system with a TruSeq SBS Kit v5 (Illumina), and the number of sequencing cycles was 2×100. The reads were mapped to the Arabidopsis reference genome (The Arabidopsis Information Resource [TAIR10]) using the Burrows-Wheeler Alignment Tool v 0.5.9 (Li and Durbin, 2009). The SNPs/InDels were prefiltered with the coverage threshold set to 10, and only those supported by at least three reads in the forward and three reads in the reverse direction were retained. Further SNP/InDel calling was done with SAMtools software (v 0.1.17, http://samtools.sourceforge.net/).

Stress Treatments

The photorespiration-promoting conditions were applied according to the procedure used for the *cat2-2* revertant screen. For stress experiments, including media change, seeds were grown on a nylon mesh (ø = 20 μM; Prosep) and transferred to specified media 3 d before the treatment. Following the onset of the treatment, the averaged numerical F_v'/F_m' values were recorded with the ImagingWin software (Heinz Walz) and plotted against the time of treatment to compare the tested lines. In parallel, color-coded images were acquired to visualize the spatial distribution of the F_v'/F_m' values. Each experiment was performed in three biological replicates.

For high-light treatment in soil, plants were grown in a controlled climate chamber (Vötsch Industrietechnik) at 3000 μL L^{-1} CO_2, 21°C, and 50% relative humidity using a 16-h-light (120 to 130 μmol m^{-2} s^{-1})/8-h-dark regime. After 21 d of growth, plants were exposed to continuous high-light (1000 μmol m^{-2} s^{-1}) illumination (Sanyo Fitotron plant growth chamber) at ambient CO_2 concentration, 21°C, and 50% relative humidity for a specified time period. Before transfer, plants were well watered to exclude the possible influence of drought.

The effect of *shr-6* on stress sensitivity was probed using mannitol (25 and 50 mM), NaCl (50 and 100 mM), and 1.5 mM H_2O_2. Wild-type (Col-0) and *shr-6* seeds were surface sterilized, cold treated for 3 d at 4°C, and sown in round Petri plates (ø = 14 cm) on 0.5× MS medium (1% [w/v] sucrose) supplemented with the chemicals described above. Plants were grown under controlled environmental conditions (16 h light [100 μmol m^{-2} s^{-1}]/8 h dark; 21°C). Every second day, starting from 5 d after germination, each plate was photographed with a fixed camera (Canon 650D body with 18 Mpx CMOS sensor, equipped with a Canon EF 35mm [f 2.0] objective) using four neon LNK.4100.8 lamps (Lyvia) as light sources, and the resulting images were used to quantify projected rosette area with an ImageJ plug-in. The averaged rosette area (n = 8) was plotted versus time to visualize the stress effect on growth kinetics.

Glutathione and Ascorbate Quantifications

Glutathione and ascorbate were assayed as described (Queval and Noctor, 2007). Briefly, ~100 mg rosette tissue was ground in 0.2 M HCl. After centrifugation at 16,000*g* for 10 min at 4°C, the supernatant was adjusted to pH 5.0 and reduced and oxidized forms of ascorbate and glutathione were quantified by plate-reader assay.

RNA-Seq Analysis

Three-week-old Col-0, *shr-6*, *cat2-2*, and *cat2-2 shr-6* plants were subjected to photorespiration-promoting conditions as described above. Shoot tissue was sampled from three biological replicates before (t = 0) and after 24 h of treatment. Each replicate consisted of at least five rosettes. RNA was extracted with TRIzol reagent and further purified with an RNeasy Kit (Qiagen) according to the manufacturer's instructions. Library preparation and sequencing were performed at the VIB Nucleomics Core. Sequencing libraries were constructed with the TruSeq Stranded mRNA Library Preparation Kit (Illumina). Three biological replicates were sequenced on Illumina NextSequation 500, resulting in ~30 million 75-bp single-end reads per sample. Adapter sequences and low-quality base pairs (Q < 20) were trimmed with Trim Galore (v0.3.3, http://www.bioinformatics.babraham.ac.uk/projects/trim_galore/), retaining high-quality reads of at least 50 bp in length. Quality-filtered reads were aligned to the TAIR10 Arabidopsis reference genome using the spliced aligner TopHat2 (v2.1.0) (Kim et al., 2013). The number of reads per gene was quantified with the featureCounts function as implemented in the Subread package v1.4.6 (Liao et al., 2014). Reads mapping to genes annotated as rRNA, tRNA, and other RNA forms (TAIR10 annotation) were not considered for further analysis.

Differentially expressed genes were identified with the R (v3.1.2) software package edgeR (Robinson et al., 2010). Genes with expression values greater than 0.12 cpm (corresponding to five read counts) in at least three samples were retained (21,127 genes). TMM normalization (Robinson and Oshlack, 2010) was applied using the calcNormFactors function. Variability in the data set was assessed with a MDSplot employing the 3000 top genes to calculate pairwise distances (top = 3000). There was a clear separation according to genotype and photorespiratory treatment, except for the *shr-6* samples, which had a less dramatic treatment separation and correlated closely to the unstressed *cat2-2 shr-6* samples. To test user-defined hypotheses, a no-intercept single-factor model was defined combining genotype and treatment factors, such as *cat-2*_photorespiratory stress. Dispersions were estimated with the estimateGLMRobustDisp function. A negative binomial regression model was used to model the overdispersed counts for each gene separately with fixed values for the dispersion parameter as outlined (McCarthy et al., 2012) and as implemented in the function glmFit using the above described model. Hypothesis testing was based on likelihood ratio tests. Contrasts of interest were the response between different genotypes under control conditions, the effect of photorespiratory stress in each genotype, and the interaction effect of photorespiratory stress and genotype at each time point. False discovery rate adjustments of the P values were performed with the method described by Benjamini and Hochberg (1995). The gene expression data were deposited in Gene Expression Omnibus (GEO; http://www.ncbi.nlm.nih.gov/geo/) under accession number GSE77017.

Identification of ROS-Responsive Genes

To generate a robust ROS signature, the raw intensity .cel files from five studies featuring ROS-generating conditions were obtained from the GEO and ArrayExpress (http://www.ebi.ac.uk/arrayexpress/). The following experiments were considered: reillumination of the conditional *flu* mutant for 2 h after a dark acclimation (GSE10812); treatment of seedlings with oligomycin for 4 h (GSE38965); treatment of seedlings with 50 μM antimycin A for 3 h (GSE41136); exposure of seedlings to ozone for 6 h (E-MEXP-342); and treatment of seedlings with 10 mM H_2O_2 for 24 h (unpublished). All raw intensity files were normalized by robust multiarray averaging with the Bioconductor package affy (v1.40.0). Probe sets were updated with the TAIR10 CDF annotation retrieved from BrainArray (TAIRG v18.0.0, http://brainarray.mbni.med.umich.edu/). Differential gene expression was analyzed with the limma package (v3.18.13) using empirical Bayes moderated t-statistics. Differentially expressed genes were selected for each transcriptomic response, using a P value of 0.01 as a significance threshold and absolute $\log_2$ fold change greater than 1.

Gas Chromatography-Mass Spectrometry Metabolite Profiling

For analysis of polar metabolites, plants were subjected to the photorespiratory stress assay as described for the *cat2-2* revertant screen. Tissue samples were collected before and after 24 h of exposure to

photorespiration-promoting conditions. For each time point, five samples (57 to 64 mg) of shoot tissue per genotype were harvested, frozen immediately in liquid nitrogen, and homogenized with a ball mill (Retsch). The powdered tissue was extracted with 300 μL methanol and 30 μL of internal standard (0.1 mg mL^{-1} ribitol) for 15 min at 70°C, after which 200 μL of chloroform was added. The samples were incubated in a rotating shaker for 5 min at 37°C, and after addition of 400 μL of water, vortexed and centrifuged for 15 min at 16,100*g*. Aliquots of the polar phase (160 μL) were dried in a vacuum concentrator (Labconco). The dried residue was redissolved and derivatized for 90 min at 30°C in 40 μL of 20 mg mL^{-1} *O*-methylhydroxyamine hydrochloride in pyridine. Next, 70 μL of *N*-methyl-*N*-(trimethylsilyl)trifluoroacetamide and 10 μL of the retention time standard *n*-alkane mixture (C12, C15, C19, C22, C28, C32, and C36) were added. The samples were incubated for 30 min at 37°C in a rotating shaker. Gas chromatography-mass spectrometry analyses were performed with a quadrupole mass-selective detector (model 5973; Hewlett-Packard), coupled to a GC system (6890 series; Hewlett-Packard) equipped with an automated sample injector and a VF-5ms capillary column (30 m × 0.25 mm) using a sample volume of 1 μL. The injector operated in a splitless mode at 230°C with a constant helium flow of 1 mL min^{-1}. The oven temperature was held at 70°C for 5 min after injection, then raised to 325°C at a rate of 5°C min^{-1}, maintained at 325°C for 1 min, and cooled down to a final temperature of 70°C at 50°C min^{-1}. The MS transfer line was set at 250°C, the MS ion source at 230°C, and the detector at 150°C, throughout the analysis. Full mass spectra were recorded by scanning the *m/z* range of 60 to 600 with a solvent delay of 7.8 min. Peaks were aligned and integrated with the xcms package (Smith et al., 2006) implemented in Bioconductor. A custom mass spectra library from the Golm Metabolome Database (Q_MSRI_ID) was imported into the AMDIS software (Stein, 1999) to annotate peaks of interest. Statistical analysis was performed in R v3.2.2. A linear model was fitted to the metabolite measurements with the lm function. Fixed effects were genotype and treatment and their interaction term. Log transformation was performed to stabilize the variance when necessary. In the case of a significant interaction term at the 5% level, all pairwise comparisons were estimated with the lsmeans package v2.21. P values were adjusted with the Tukey adjustment method. In the absence of a significant interaction term, the model was reduced and pairwise comparisons were performed between the levels of the main effects only.

Gas Exchange

For gas exchange measurements, plants were grown in 55-mm square Petri dishes, as described for the *cat2-2* revertant screen, at a density of five plants per plate. After 3 weeks of growth, lids were removed and whole plates were analyzed with the LI-6400XT portable photosynthesis system equipped with the tightly sealed Licor 6400-17 whole-plant Arabidopsis chamber and the Licor 6400-18 RGB light source. Parameters used for the measurement were as follows: light intensity, 100 μmol m^{-2} s^{-1}; CO_2 level, 400 μmol M^{-1}; ambient temperature, 23°C; flow 400 μmol s^{-1}; and stomatal ratio set to 1. After the measurements, for each plate, the fresh weight of rosettes was determined with an analytical balance.

Confocal Microscopy

For the observation of the peroxisomal behavior, plants were grown on vertical plates with 1× MS with or without sucrose for 7 d at 21°C under LD conditions. An inverted confocal microscope (Zeiss 710; objective: 40× water immersion) was used, while the region of interest was excited with an argon laser at 488 nm. The GFP emission (Pro35S:PTS1:GFP) was captured between 515 and 545 nm. To distinguish between autofluorescence of chloroplasts and GFP, a second channel collected the emitted light between 560 and 650 nm. The imaging included Z-Stack and time-lapse mode. The image processing was done with the ZEN 2009 software (Zeiss).

Accession Numbers

Sequence data for genes used in this study can be found in the Arabidopsis Genome Initiative or GenBank/EMBL databases under the following accession numbers: locus identifiers: CATALASE2 (At4g35090), SHORTROOT (At4G37650), SCARECROW (At3g54220), GLYCOLATE OXIDASE1 (At3g14420), GLYCOLATE OXIDASE2 (At3g14415), ABSCISIC ACID INSENSITIVE4 (At2g40220), NUTCRACKER (At5g44160), and BASIC LEUCINE-ZIPPER2 (At2g18160). GEO (http://www.ncbi.nlm.nih.gov/geo/) accession numbers are GSE77017 (RNA-seq data generated in this study), GSE10812 (reillumination of the conditional *flu* mutant for 2 h after a dark acclimation), GSE38965 (treatment of seedlings with oligomycin for 4 h), and GSE41136 (treatment of seedlings with 50 μM antimycin A for 3 h). ArrayExpress (http://www.ebi.ac.uk/arrayexpress/) accession number is E-MEXP-342 (exposure of seedlings to ozone for 6 h). Mutant lines are as follows: *cat2-2* (Col-0 background; SALK_057998; NASC stock no. N557998), *cat2-20* (L*er*-0 background; ET8347; http://genetrap.cshl.edu), *shr-6* (Col-0 background; SALK_002744, NASC stock no. N502744), *shr-2* (Col-0 (*gl1*) background, NASC stock no. N2972), *scr-3* (Col-0 background; NASC stock no. N3997), *scr-1* (Ws-2 background, NASC stock no. N8539), and *abi4-102* (Col-0 background, NASC stock no. N3837).

Supplemental Data

Supplemental Figure 1. Representative photograph illustrating a *cat2-2* revertant identified during the primary forward screening.

Supplemental Figure 2. Phenotype of heterozygous *shr* mutants exposed to photorespiration-promoting conditions.

Supplemental Figure 3. Phenotype of two independent *shr* alleles (*shr-6* and *shr-2*) under photorespiration-promoting conditions.

Supplemental Figure 4. Influence of exogenous sucrose supplementation on growth and development of SHR-deficient plants in vitro.

Supplemental Figure 5. Peroxisomal targeting signal1 (PTS1; Pro35S:PTS1:GFP) localization in rosette leaves of 7-d-old Col-0 and *shr-6* seedlings.

Supplemental Figure 6. Effect of photorespiration-promoting conditions on *cat2-2 abi4-102* double mutants.

Supplemental Figure 7. Comparison of the transcriptome profiles under control conditions for *shr-6*, *cat2-2*, and *cat2-2 shr-6* double mutant.

Supplemental Figure 8. Transcript abundance of genes encoding enzymes from the L-galactose pathway for ascorbic acid biosynthesis.

Supplemental Figure 9. Myo-inositol content in rosettes of 3-week-old Col-0, *cat2-2*, *shr-6*, and *cat2-2 shr-6* plants.

Supplemental Figure 10. Effect of stress treatments (50 and 100 mM NaCl, 50 and 100 mM mannitol, and 1.5 mM H_2O_2) on *shr-6* growth.

Supplemental Figure 11. Characterization of the CAT2-deficient L*er*-0 mutant (*cat2-20*).

Supplemental Table 1. List of primers and restriction enzymes used in this study.

Supplemental Data Set 1. Differential gene expression in Col-0, *cat2-2*, *shr-6*, and *cat2-2 shr-6* under control and photorespiration-promoting conditions.

Supplemental Data Set 2. List of ROS-responsive transcripts.

Supplemental Data Set 3. Differential expression of photorespiration-related genes in Col-0, *cat2-2*, *shr-6*, and *cat2-2 shr-6* under control and photorespiration-promoting conditions.

Supplemental Data Set 4. List of EMS-specific mutations in the *378.3* mutant.

ACKNOWLEDGMENTS

We thank Brigitte van de Cotte and Michaël Vandorpe for technical assistance and Martine De Cock and Annick Bleys for help in preparing the manuscript. This work was supported by grants from the Ghent University Multidisciplinary Research Partnership "Sustainable BioEconomy" (project 01MRB510W), the Interuniversity Attraction Poles Program (IUAP P7/29) initiated by the Belgian State, Science Policy Office, the Research Foundation-Flanders (grant no. G0D7914N), and Scientific Exchange program Flanders-France (grant Tournesol T.2008.21 to F.V.B and G.N.), and also partially by the Academy of Finland Centre of Excellence Program (2014-2019). C.W. is indebted to the VIB International PhD Program for a predoctoral fellowship, and P.I.K. and R.P.K. are recipients of Omics@VIB Marie Curie COFUND fellowships.

AUTHOR CONTRIBUTIONS

C.W., P.I.K., P.M., F.A.H., J.D., K.V.D.K., G.N., J.M., and F.V.B. designed the research. C.W., P.I.K., P.M., F.A.H., K.V.D.K., A.M., J.D., and R.P.K., performed research. C.W., P.I.K., P.M., F.A.H., K.V.D.K., A.M., P.W., J.D., and F.V.B. analyzed data. C.W., P.I.K., K.V.D.K., G.N., J.M., and F.V.B. wrote the article.

Received January 21, 2016; revised May 27, 2016; accepted July 11, 2016; published July 18, 2016.

REFERENCES

Baena-González, E., Rolland, F., Thevelein, J.M., and Sheen, J. (2007). A central integrator of transcription networks in plant stress and energy signalling. Nature **448:** 938–942.

Benfey, P.N., Linstead, P.J., Roberts, K., Schiefelbein, J.W., Hauser, M.T., and Aeschbacher, R.A. (1993). Root development in *Arabidopsis*: four mutants with dramatically altered root morphogenesis. Development **119:** 57–70.

Benjamini, Y., and Hochberg, Y. (1995). Controlling the false discovery rate: a practical and powerful approach to multiple testing. J. R. Stat. Soc. Ser. B Stat. Methodol. **57:** 289–300.

Bienert, G.P., Møller, A.L.B., Kristiansen, K.A., Schulz, A., Møller, I.M., Schjoerring, J.K., and Jahn, T.P. (2007). Specific aquaporins facilitate the diffusion of hydrogen peroxide across membranes. J. Biol. Chem. **282:** 1183–1192.

Chaouch, S., Queval, G., Vanderauwera, S., Mhamdi, A., Vandorpe, M., Langlois-Meurinne, M., Van Breusegem, F., Saindrenan, P., and Noctor, G. (2010). Peroxisomal hydrogen peroxide is coupled to biotic defense responses by ISOCHORISMATE SYNTHASE1 in a daylength-related manner. Plant Physiol. **153:** 1692–1705.

Chaouch, S., and Noctor, G. (2010). Myo-inositol abolishes salicylic acid-dependent cell death and pathogen defence responses triggered by peroxisomal hydrogen peroxide. New Phytol. **188:** 711–718.

Clare, D.A., Duong, M.N., Darr, D., Archibald, F., and Fridovich, I. (1984). Effects of molecular oxygen on detection of superoxide radical with nitroblue tetrazolium and on activity stains for catalase. Anal. Biochem. **140:** 532–537.

Considine, M.J., and Foyer, C.H. (2014). Redox regulation of plant development. Antioxid. Redox Signal. **21:** 1305–1326.

Cui, H., Hao, Y., and Kong, D. (2012). SCARECROW has a SHORT-ROOT-independent role in modulating the sugar response. Plant Physiol. **158:** 1769–1778.

Cui, H., Hao, Y., Kovtun, M., Stolc, V., Deng, X.-W., Sakakibara, H., and Kojima, M. (2011). Genome-wide direct target analysis reveals a role for SHORT-ROOT in root vascular patterning through cytokinin homeostasis. Plant Physiol. **157:** 1221–1231.

Cui, H., Kong, D., Liu, X., and Hao, Y. (2014). SCARECROW, SCR-LIKE 23 and SHORT-ROOT control bundle sheath cell fate and function in *Arabidopsis thaliana.* Plant J. **78:** 319–327.

Cui, H., Levesque, M.P., Vernoux, T., Jung, J.W., Paquette, A.J., Gallagher, K.L., Wang, J.Y., Blilou, I., Scheres, B., and Benfey, P.N. (2007). An evolutionarily conserved mechanism delimiting SHR movement defines a single layer of endodermis in plants. Science **316:** 421–425.

Dhondt, S., Coppens, F., De Winter, F., Swarup, K., Merks, R.M.H., Inzé, D., Bennett, M.J., and Beemster, G.T.S. (2010). SHORT-ROOT and SCARECROW regulate leaf growth in Arabidopsis by stimulating S-phase progression of the cell cycle. Plant Physiol. **154:** 1183–1195.

Di Laurenzio, L., Wysocka-Diller, J., Malamy, J.E., Pysh, L., Helariutta, Y., Freshour, G., Hahn, M.G., Feldmann, K.A., and Benfey, P.N. (1996). The *SCARECROW* gene regulates an asymmetric cell division that is essential for generating the radial organization of the Arabidopsis root. Cell **86:** 423–433.

Donahue, J.L., Alford, S.R., Torabinejad, J., Kerwin, R.E., Nourbakhsh, A., Ray, W.K., Hernick, M., Huang, X., Lyons, B.M., Hein, P.P., and Gillaspy, G.E. (2010). The *Arabidopsis thaliana myo*-inositol 1-phosphate synthase1 gene is required for *myo*-inositol synthesis and suppression of cell death. Plant Cell **22:** 888–903.

Endres, S., and Tenhaken, R. (2009). Myoinositol oxygenase controls the level of myoinositol in Arabidopsis, but does not increase ascorbic acid. Plant Physiol. **149:** 1042–1049.

Foyer, C.H., and Noctor, G. (2009). Redox regulation in photosynthetic organisms: signaling, acclimation, and practical implications. Antioxid. Redox Signal. **11:** 861–905.

Fukaki, H., Fujisawa, H., and Tasaka, M. (1996). *SGR1*, *SGR2*, and *SGR3*: novel genetic loci involved in shoot gravitropism in *Arabidopsis thaliana*. Plant Physiol. **110:** 945–955.

Fukaki, H., Wysocka-Diller, J., Kato, T., Fujisawa, H., Benfey, P.N., and Tasaka, M. (1998). Genetic evidence that the endodermis is essential for shoot gravitropism in *Arabidopsis thaliana.* Plant J. **14:** 425–430.

Gadjev, I., Vanderauwera, S., Gechev, T.S., Laloi, C., Minkov, I.N., Shulaev, V., Apel, K., Inzé, D., Mittler, R., and Van Breusegem, F. (2006). Transcriptomic footprints disclose specificity of reactive oxygen species signaling in Arabidopsis. Plant Physiol. **141:** 436–445.

Gardiner, J., Donner, T.J., and Scarpella, E. (2011). Simultaneous activation of *SHR* and *ATHB8* expression defines switch to preprocambial cell state in Arabidopsis leaf development. Dev. Dyn. **240:** 261–270.

Hayashi, M., Toriyama, K., Kondo, M., and Nishimura, M. (1998). 2,4-Dichlorophenoxybutyric acid-resistant mutants of Arabidopsis have defects in glyoxysomal fatty acid β-oxidation. Plant Cell **10:** 183–195.

Helariutta, Y., Fukaki, H., Wysocka-Diller, J., Nakajima, K., Jung, J., Sena, G., Hauser, M.-T., and Benfey, P.N. (2000). The *SHORT-ROOT* gene controls radial patterning of the *Arabidopsis* root through radial signaling. Cell **101:** 555–567.

Jacques, S., Ghesquière, B., De Bock, P.-J., Demol, H., Wahni, K., Willems, P., Messens, J., Van Breusegem, F., and Gevaert, K. (2015). Protein methionine sulfoxide dynamics in *Arabidopsis thaliana* under oxidative stress. Mol. Cell. Proteomics **14:** 1217–1229.

Kaurilind, E., Xu, E., and Brosché, M. (2015). A genetic framework for H_2O_2 induced cell death in *Arabidopsis thaliana*. BMC Genomics **16:** 837.

Kerchev, P., Mühlenbock, P., Denecker, J., Morreel, K., Hoeberichts, F.A., Van Der Kelen, K., Vandorpe, M., Nguyen, L., Audenaert, D., and Van Breusegem, F. (2015). Activation of auxin signalling counteracts photorespiratory H_2O_2-dependent cell death. Plant Cell Environ. **38:** 253–265.

Kim, D., Pertea, G., Trapnell, C., Pimentel, H., Kelley, R., and Salzberg, S.L. (2013). TopHat2: accurate alignment of transcriptomes in the presence of insertions, deletions and gene fusions. Genome Biol. **14:** R36.

Laby, R.J., Kincaid, M.S., Kim, D., and Gibson, S.I. (2000). The *Arabidopsis* sugar-insensitive mutants *sis4* and *sis5* are defective in abscisic acid synthesis and response. Plant J. **23:** 587–596.

Laing, W.A., Ogren, W.L., and Hageman, R.H. (1974). Regulation of soybean net photosynthetic CO_2 fixation by the interaction of CO_2, O_2, and ribulose 1,5-diphosphate carboxylase. Plant Physiol. **54:** 678–685.

Levesque, M.P., Vernoux, T., Busch, W., Cui, H., Wang, J.Y., Blilou, I., Hassan, H., Nakajima, K., Matsumoto, N., Lohmann, J.U., Scheres, B., and Benfey, P.N. (2006). Whole-genome analysis of the SHORT-ROOT developmental pathway in *Arabidopsis.* PLoS Biol. **4:** e143.

Liao, Y., Smyth, G.K., and Shi, W. (2014). featureCounts: an efficient general purpose program for assigning sequence reads to genomic features. Bioinformatics **30:** 923–930.

Li, H., and Durbin, R. (2009). Fast and accurate short read alignment with Burrows-Wheeler transform. Bioinformatics **25:** 1754–1760.

Li, S., Mhamdi, A., Trotta, A., Kangasjärvi, S., and Noctor, G. (2014). The protein phosphatase subunit PP2A-B'γ is required to suppress day length-dependent pathogenesis responses triggered by intracellular oxidative stress. New Phytol. **202:** 145–160.

Lorence, A., Chevone, B.I., Mendes, P., and Nessler, C.L. (2004). Myo-inositol oxygenase offers a possible entry point into plant ascorbate biosynthesis. Plant Physiol. **134:** 1200–1205.

Mateo, A., Mühlenbock, P., Rustérucci, C., Chang, C.C.-C., Miszalski, Z., Karpińska, B., Parker, J.E., Mullineaux, P.M., and Karpiński, S. (2004). *LESION SIMULATING DISEASE 1* is required for acclimation to conditions that promote excess excitation energy. Plant Physiol. **136:** 2818–2830.

McCarthy, D.J., Chen, Y., and Smyth, G.K. (2012). Differential expression analysis of multifactor RNA-Seq experiments with respect to biological variation. Nucleic Acids Res. **40:** 4288–4297.

Mhamdi, A., Queval, G., Chaouch, S., Vanderauwera, S., Van Breusegem, F., and Noctor, G. (2010). Catalase function in plants: a focus on *Arabidopsis* mutants as stress-mimic models. J. Exp. Bot. **61:** 4197–4220.

Mhamdi, A., Noctor, G., and Baker, A. (2012). Plant catalases: peroxisomal redox guardians. Arch. Biochem. Biophys. **525:** 181–194.

Mittler, R., Vanderauwera, S., Suzuki, N., Miller, G., Tognetti, V.B., Vandepoele, K., Gollery, M., Shulaev, V., and Van Breusegem, F. (2011). ROS signaling: the new wave? Trends Plant Sci. **16:** 300–309.

Mukherjee, M., Larrimore, K.E., Ahmed, N.J., Bedick, T.S., Barghouthi, N.T., Traw, M.B., and Barth, C. (2010). Ascorbic acid deficiency in *Arabidopsis* induces constitutive priming that is dependent on hydrogen peroxide, salicylic acid, and the NPR1 gene. Mol. Plant-Microbe Interact. **23:** 340–351.

Nakajima, K., Sena, G., Nawy, T., and Benfey, P.N. (2001). Intercellular movement of the putative transcription factor SHR in root patterning. Nature **413:** 307–311.

Neff, M.M., Turk, E., and Kalishman, M. (2002). Web-based primer design for single nucleotide polymorphism analysis. Trends Genet. **18:** 613–615.

Nito, K., Kamigaki, A., Kondo, M., Hayashi, M., and Nishimura, M. (2007). Functional classification of *Arabidopsis* peroxisome biogenesis factors proposed from analyses of knockdown mutants. Plant Cell Physiol. **48:** 763–774.

Noctor, G., Lelarge-Trouverie, C., and Mhamdi, A. (2015). The metabolomics of oxidative stress. Phytochemistry **112:** 33–53.

Peterhansel, C., and Maurino, V.G. (2011). Photorespiration redesigned. Plant Physiol. **155:** 49–55.

Queval, G., Issakidis-Bourguet, E., Hoeberichts, F.A., Vandorpe, M., Gakière, B., Vanacker, H., Miginiac-Maslow, M., Van Breusegem, F., and Noctor, G. (2007). Conditional oxidative stress responses in the Arabidopsis photorespiratory mutant *cat2* demonstrate that redox state is a key modulator of daylength-dependent gene expression, and define photoperiod as a crucial factor in the regulation of H_2O_2-induced cell death. Plant J. **52:** 640–657.

Queval, G., and Noctor, G. (2007). A plate reader method for the measurement of NAD, NADP, glutathione, and ascorbate in tissue extracts: Application to redox profiling during Arabidopsis rosette development. Anal. Biochem. **363:** 58–69.

Robinson, M.D., McCarthy, D.J., and Smyth, G.K. (2010). edgeR: a Bioconductor package for differential expression analysis of digital gene expression data. Bioinformatics **26:** 139–140.

Robinson, M.D., and Oshlack, A. (2010). A scaling normalization method for differential expression analysis of RNA-seq data. Genome Biol. **11:** R25.

Rojas, C.M., Senthil-Kumar, M., Wang, K., Ryu, C.-M., Kaundal, A., and Mysore, K.S. (2012). Glycolate oxidase modulates reactive oxygen species-mediated signal transduction during nonhost resistance in *Nicotiana benthamiana* and *Arabidopsis.* Plant Cell **24:** 336–352.

Sandalio, L.M., and Romero-Puertas, M.C. (2015). Peroxisomes sense and respond to environmental cues by regulating ROS and RNS signalling networks. Ann. Bot. (Lond.) **116:** 475–485.

Scheres, B., Di Laurenzio, L., Willemsen, V., Hauser, M.-T., Janmaat, K., Weisbeek, P., and Benfey, P.N. (1995). Mutations affecting the radial organisation of the *Arabidopsis* root display specific defects throughout the embryonic axis. Development **121:** 53–62.

Schneeberger, K., Ossowski, S., Lanz, C., Juul, T., Petersen, A.H., Nielsen, K.L., Jørgensen, J.E., Weigel, D., and Andersen, S.U. (2009). SHOREmap: simultaneous mapping and mutation identification by deep sequencing. Nat. Methods **6:** 550–551.

Schürmann, P., and Buchanan, B.B. (2008). The ferredoxin/thioredoxin system of oxygenic photosynthesis. Antioxid. Redox Signal. **10:** 1235–1274.

Slewinski, T.L., Anderson, A.A., Zhang, C., and Turgeon, R. (2012). *Scarecrow* plays a role in establishing Kranz anatomy in maize leaves. Plant Cell Physiol. **53:** 2030–2037.

Smith, C.A., Want, E.J., O'Maille, G., Abagyan, R., and Siuzdak, G. (2006). XCMS: processing mass spectrometry data for metabolite profiling using nonlinear peak alignment, matching, and identification. Anal. Chem. **78:** 779–787.

Somerville, C.R., and Ogren, W.L. (1979). A phosphoglycolate phosphatase-deficient mutant of *Arabidopsis.* Nature **280:** 833–836.

Stein, S.E. (1999). An integrated method for spectrum extraction and compound identification from gas chromatography/mass spectrometry data. J. Am. Soc. Mass Spectrom. **10:** 770–781.

Sundaresan, V., Springer, P., Volpe, T., Haward, S., Jones, J.D., Dean, C., Ma, H., and Martienssen, R. (1995). Patterns of gene action in plant development revealed by enhancer trap and gene trap transposable elements. Genes Dev. **9:** 1797–1810.

Tian, S., Wang, X., Li, P., Wang, H., Ji, H., Xie, J., Qiu, Q., Shen, D., and Dong, H. (2016). Plant aquaporin AtPIP1;4 links apoplastic H_2O_2 induction to disease immunity pathways. Plant Physiol. **171:** 1635–1650.

Timm, S., and Bauwe, H. (2013). The variety of photorespiratory phenotypes – employing the current status for future research directions on photorespiration. Plant Biol (Stuttg) **15:** 737–747.

Van den Ende, W., and Valluru, R. (2009). Sucrose, sucrosyl oligosaccharides, and oxidative stress: scavenging and salvaging? J. Exp. Bot. **60:** 9–18.

Vandenabeele, S., Vanderauwera, S., Vuylsteke, M., Rombauts, S., Langebartels, C., Seidlitz, H.K., Zabeau, M., Van Montagu, M., Inzé, D., and Van Breusegem, F. (2004). Catalase deficiency drastically affects gene expression induced by high light in *Arabidopsis thaliana*. Plant J. **39:** 45–58.

Vanderauwera, S., Suzuki, N., Miller, G., van de Cotte, B., Morsa, S., Ravanat, J.-L., Hegie, A., Triantaphylidès, C., Shulaev, V., Van Montagu, M.C.E., Van Breusegem, F., and Mittler, R. (2011). Extranuclear protection of chromosomal DNA from oxidative stress. Proc. Natl. Acad. Sci. USA **108:** 1711–1716.

Vanderauwera, S., Vandenbroucke, K., Inzé, A., van de Cotte, B., Mühlenbock, P., De Rycke, R., Naouar, N., Van Gaever, T., Van Montagu, M.C.E., and Van Breusegem, F. (2012). AtWRKY15 perturbation abolishes the mitochondrial stress response that steers osmotic stress tolerance in *Arabidopsis.* Proc. Natl. Acad. Sci. USA **109:** 20113–20118.

Vanderauwera, S., Zimmermann, P., Rombauts, S., Vandenabeele, S., Langebartels, C., Gruissem, W., Inzé, D., and Van Breusegem, F. (2005). Genome-wide analysis of hydrogen peroxide-regulated gene expression in Arabidopsis reveals a high light-induced transcriptional cluster involved in anthocyanin biosynthesis. Plant Physiol. **139:** 806–821.

Wang, P., Kelly, S., Fouracre, J.P., and Langdale, J.A. (2013). Genome-wide transcript analysis of early maize leaf development reveals gene cohorts associated with the differentiation of C4 Kranz anatomy. Plant J. **75:** 656–670.

Waszczak, C., et al. (2014). Sulfenome mining in *Arabidopsis thaliana.* Proc. Natl. Acad. Sci. USA **111:** 11545–11550.

Waszczak, C., Akter, S., Jacques, S., Huang, J., Messens, J., and Van Breusegem, F. (2015). Oxidative post-translational modifications of cysteine residues in plant signal transduction. J. Exp. Bot. **66:** 2923–2934.

Welch, D., Hassan, H., Blilou, I., Immink, R., Heidstra, R., and Scheres, B. (2007). *Arabidopsis* JACKDAW and MAGPIE zinc finger proteins delimit asymmetric cell division and stabilize tissue boundaries by restricting SHORT-ROOT action. Genes Dev. **21:** 2196–2204.

Widholm, J.M., and Ogren, W.L. (1969). Photorespiratory-induced senescence of plants under conditions of low carbon dioxide. Proc. Natl. Acad. Sci. USA **63:** 668–675.

Yu, N.I., Lee, S.A., Lee, M.-H., Heo, J.-O., Chang, K.S., and Lim, J. (2010). Characterization of SHORT-ROOT function in the *Arabidopsis* root vascular system. Mol. Cells **30:** 113–119.

Zolman, B.K., and Bartel, B. (2004). An *Arabidopsis* indole-3-butyric acid-response mutant defective in PEROXIN6, an apparent ATPase implicated in peroxisomal function. Proc. Natl. Acad. Sci. USA **101:** 1786–1791.